ACS Sustainable Chemistry & Engineering

pubs.acs.org/journal/ascecg

Research Article

Boosting the Chemical Hydrogenolysis of Glycerol to 1,2-Propanediol to Almost Perfect Selectivity Using a Multifunctional Ru−Cu Carbon-Nanotube-Supported Catalyst

Piet Hassenstein, Daniel Niehaus, Nazanin Taherkhani, Jan-Dominik H. Krueger, Dorothea Voß, Dominique Lumpp, Baldur Schroeter, Leandros Paschalidis, Irina Smirnova, Mirko Skiborowski, and Jakob Albert*

Cite This: https://doi.org/10.1021/acssuschemeng.6c02083

Read Online

ACCESS | Metrics & More | Article Recommendations | Supporting Information

ABSTRACT: Chemical hydrogenolysis of glycerol to propanediols is a promising strategy for biomass valorization. However, the demanding reaction conditions and deviating requirements for the individual reaction steps cause significant challenges to date. Herein, a kinetic study for the chemical hydrogenolysis of glycerol to 1,2-propanediol (1,2-PDO) as well as an optimized reaction procedure using a multifunctional Ru−Cu/CNT catalyst is presented. In detail, it was shown that the glycerol hydrogenolysis reaction is neither influenced by mass nor heat transfer limitations under the applied reaction conditions. Consequently, the following kinetic parameters could be deduced both by experimental determination as well as kinetic modeling: n (glycerol) = 1.1, n (H_2) = 0.12 up to 25 bar (kinetic regime), and an activation energy of 150 kJ mol^{-1} for the desired 1,2-PDO pathway, as well as n (glycerol) = n (H_2) = 0 for the undesired ethylene glycol pathway at an activation energy of around 65 kJ mol^{-1}. Moreover, separating glycerol hydrogenolysis into two steps, initial glycerol dehydration to acetol under a nitrogen atmosphere at a high temperature of 220 °C, followed by acetol hydrogenation to 1,2-PDO under a hydrogen atmosphere at a low temperature of 145 °C using the same Ru−Cu/CNT catalyst, can lead to higher overall yields and almost perfect selectivity for 1,2-PDO. This could be verified in a separate experiment showing acetol selectivity of >99% for the first and 1,2-PDO selectivity of >99% for the second step without observable ethylene glycol production. Compared to the combined reaction under standard hydrogenolysis conditions of 50 bar H_2 and 220 °C, almost perfect 1,2-PDO selectivity could be achieved, showing great potential for the separate approach. Moreover, a kinetic model of the glycerol hydrogenolysis based on the experimentally derived reaction rates confirms that the models reliably reproduce the observed reaction behavior with respect to the observed kinetic parameters.

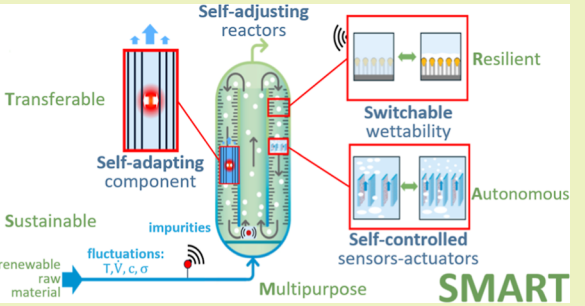

KEYWORDS: *glycerol hydrogenolysis, 1,2-propanediol, kinetics, multifunctional catalyst, carbon nanotubes*

INTRODUCTION

As the reduction of greenhouse gas emissions becomes increasingly important, the production of alternative green fuels is gaining more relevance. Biodiesel, produced through the transesterification of triglycerides with methanol, is an alternative fuel that is growing in importance. As biodiesel production increases over time, the production of biobased glycerol as a byproduct also increases, thereby reducing its price. This price drop enables the use of glycerol for applications that were previously not economically viable.[1]

One such application is the use as a cheap, biobased chemical platform to produce higher-value products, such as acrolein,[2] 1,3-propandiol,[3] and 1,2-propanediol (1,2-PDO).[4−6] 1,2-PDO is used as a monomer for polymer resins or as an additive in pharmaceuticals, cosmetics, food, and animal feed. However, there are challenges in using biobased glycerol as a substrate that must be overcome. For example, the crude glycerol produced by the biodiesel industry contains significant impurities, such as water, ash, and soap, which can account for 20−40% of its weight.[7] This challenge can be overcome either by purification of the crude glycerol or by developing a process that is unaffected by the contaminants.

The conventional production of 1,2-PDO through the hydration of propylene oxide, which typically occurs at 190 °C and 18 bar, utilizes 6.25% propylene oxide in water and requires an additional distillation step to separate 1,2-PDO.[8] A newly established 1,2-PDO production process based on

Received: February 18, 2026
Revised: March 19, 2026
Accepted: March 20, 2026

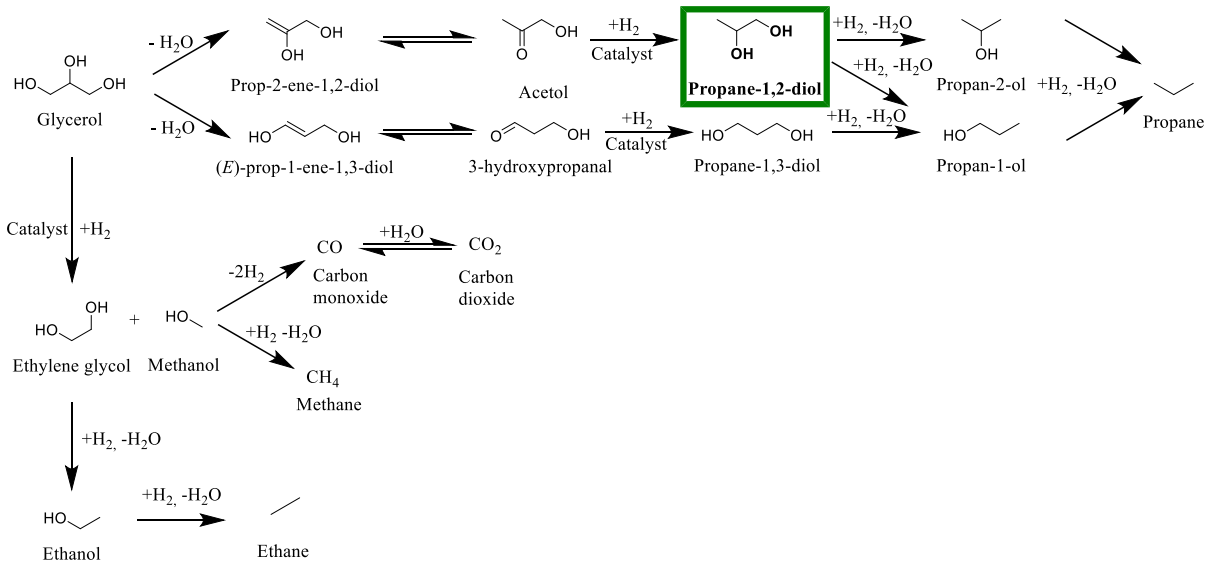

Figure 1. General reaction scheme of the hydrogenolysis of glycerol and side reactions at T = 160−260 °C and p = 40−100 bar hydrogen pressure, with the desired product 1,2-PDO highlighted in green.[10,11]

glycerol hydrogenolysis would not only be more sustainable due to the use of biobased feedstock but also might be able to use a higher reactant concentration, requiring less energy-consuming purification methods.[7,9]

The hydrogenolysis of glycerol to 1,2-PDO is a three-step reaction, as illustrated in Figure 1, which shows the entire reaction network including several parallel and consecutive reactions, adapted from Gatti et al.[10] and Dasari et al.[11]

The first step involves dehydration of glycerol to prop-2-en-1,2-diol, which immediately rearranges via keto−enol tautomerization during the second step to acetol. In the third step, acetol is hydrogenated to 1,2-PDO using a hydrogenation catalyst.[11] Following this, a consecutive hydrogenolysis to monohydroxy alcohols and finally to propane is possible and needs to be suppressed.[12] The dehydration at a secondary glycerol hydroxy group is possible and must be avoided. The formed (E)-prop-1-ene-1,3-diol undergoes an analogous path as prop-2-en-1,2-diol to form propane-1,3-diol. Finally, the C−C cleavage of glycerol to form C1 and C2 products, such as methanol and ethylene glycol, must also be prevented. Ethylene glycol can further undergo hydrogenolysis to form ethanol and subsequently ethane, while methanol can be further decomposed to carbon monoxide or carbon dioxide.[12]

Therefore, reaction conditions that favor the kinetically preferred primary dehydration over the thermodynamically favored secondary dehydration and prevent subsequent hydrogenolysis and the C−C-cleavage of glycerol to ethylene glycol must be identified.[13]

Several different carbon-supported heterogeneous metal catalysts, including Ru,[6,14−16] Rh,[17] Ni,[18−20] Pt,[21−23] and Cu[11,24−26] have been investigated for their ability to catalyze glycerol hydrogenolysis, with Ru proving the most effective. Wang et al.[27] noted that Ru-based catalysts supported on monoclinic zirconia exhibit a higher turnover rate compared to Rh-, Pt-, and Pd-based catalysts. However, Ru-based catalysts tend to catalyze C−C cleavage, reducing the selectivity. For example, one Ru/C catalyst demonstrated a 68% selectivity toward ethylene glycol, while only 32% of the product was 1,2-PDO.[28]

Sherbi et al.[29] were able to overcome Ru's tendency to catalyze the C−C cleavage by creating a bimetallic Ru−Cu catalyst supported on multiwall carbon nanotubes (CNTs) via a wetness impregnation method. Adding copper promoted C−O cleavage over C−C cleavage, which is catalyzed by purely Ru-based catalysts. This resulted in a high selectivity for 1,2-PDO of up to 93.4%.

Hydrogenolysis of 1,2-PDO using a bimetallic (Ru−Re) catalyst supported on activated carbon, with hydrogen pressures up to 100 bar, was found to be completely kinetically controlled with minimal mass transport limitations and selectivity for 1,2-PDO of up to 36.6%.[30] For both Cu/SiO_2 and Cu/ZrO_2 catalysts, nearly zero-order dependence on glycerol concentration and first-order dependence on hydrogen concentration were found, while achieving selectivities of up to 95% and 36.6%, respectively.[31,32] However, not all Cu-based catalysts exhibit a zero-reaction order for glycerol. For example, both Cu/MgO and $CuPd/TiO_2$ catalysts exhibited a higher dependence on glycerol concentration, with reaction orders of 1.2 and 0.9, respectively.[33,34]

Gabrysch et al.[32] observed that hydrogen acts hereby in a dual role. First, it serves as a reactant and creates empty adsorption sites on the catalyst surface. By removing elemental oxygen originating from water adsorption, hydrogen enables the dissociative adsorption of glycerol. In addition, they found that increasing hydrogen pressure up to 25 bar decreases 1,2-PDO selectivity due to increased formation of ethylene glycol by C−C cleavage.

However, the reaction rate is not universally independent of the glycerol concentration for Cu-based catalysts. A pseudo-first-order dependence on glycerol was reported for a Cu/Zn:Cr/Zr mixed metal oxide catalyst by Sharma et al.[35]

While previous experiments were conducted as single-batch experiments combining all reaction steps in a single slurry reactor, Chiu et al.[36] proposed an alternative process, which should result in higher 1,2-PDO selectivity. This was achieved by separating the glycerol dehydration and acetol hydrogenation steps in two separate vessels. Using a Cu-Chromite catalyst, they conducted the dehydration of glycerol to acetol via reactive distillation, achieving over 90% glycerol conversion

https://doi.org/10.1021/acssuschemeng.6c02083
ACS Sustainable Chem. Eng. XXXX, XXX, XXX−XXX

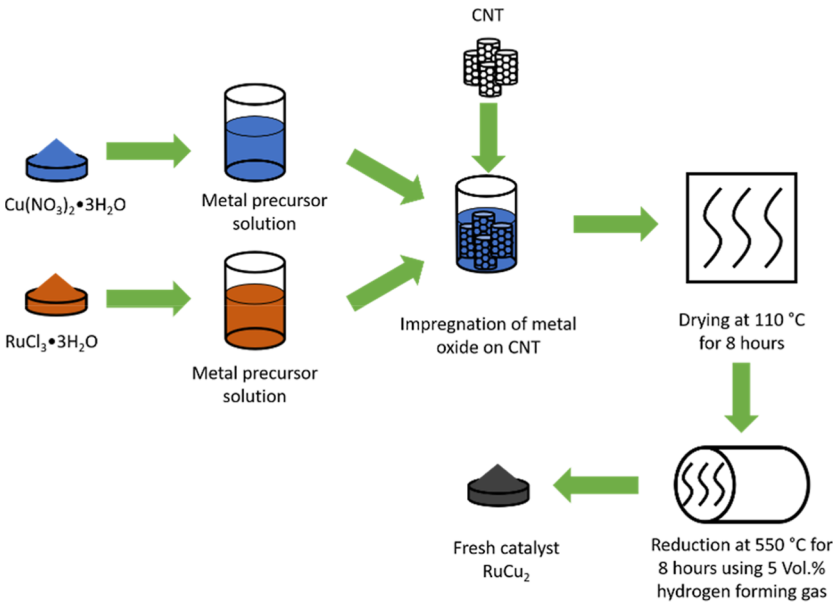

Figure 2. Schematic representation of the catalyst preparation using the wetness impregnation method.[29]

and a high acetol selectivity. However, they did not further hydrogenate acetol to 1,2-PDO.

While various supports have been used for Ru-based catalysts, such as Al_2O_3,[37] SiO_2,[38] ZrO_2,[39] and TiO_2,[40] Gatti et al.[41] note in their review that carbon-based supports are superior, providing the necessary high specific surface area to disperse metal particles effectively, thereby increasing activity. Moreover, the authors note that carbon-based supports tend to exhibit higher stability and do not undergo hydrothermal alterations compared to traditional metal oxide supports.[41] Comparing various carbon supports, Ru-based catalysts tend to be more active if supported on CNTs rather than on active carbon, due to an increased amount of the electron-rich $Ru^{\delta-}$ species, which favors the terminal C−O bond cleavage.[42]

In this study, a Ru−Cu/CNT catalyst, previously developed and characterized by Lumpp et al.[43] is used to catalyze the glycerol hydrogenolysis reaction. To the best of our knowledge, this is the first detailed kinetic study of a bimetallic CNT-supported Ru−Cu catalyst for the chemical hydrogenolysis of glycerol to 1,2-PDO. As previous studies have shown, the influence of reaction conditions on kinetics varies depending on the used catalyst, and on occasion, these are even contradictory.[30−35] Therefore, it is necessary to determine the impact of all reaction parameters for each new catalyst to understand and fully reveal the reaction mechanism and key intermediates. In order to guarantee that the determined kinetic parameters are not influenced by mass or heat transfer limitations, these influences must be checked first. Afterward, temperature, glycerol concentration, initial hydrogen pressure, and catalyst loading and their impact on the reaction rate will be varied in order to determine the key kinetic parameters. In addition, the individual subreactions of the reaction network are investigated to determine which occur under the applied conditions, which are rate-determining, and which are even favored. Studying the individual subreactions is necessary to find reaction conditions that suppress undesired side reactions, especially C−C cleavage. Furthermore, this study aims to improve not only the reaction conditions but also the entire process and provide a foundation for the design of a future SMART (sustainable, multipurpose, autonomous, resilient, transferable) glycerol hydrogenolysis reactor. When combined with catalyst development and process optimization, this reactor will overcome challenges associated with biobased glycerol feedstock.

EXPERIMENTAL SECTION

Materials

All materials were purchased and used without further purification, except for the catalyst. The Ru−Cu/CNT catalyst was synthesized using an improved wetness impregnation method based on the work of Sherbi et al.[29] Multiwalled NANOCYL NC7000 carbon nanotubes by Nanocyl SA., Belgium, which is a nanoparticle powder widely applied in industrial scale CNT-modified material as well as $RuCl_3 \cdot 3H_2O$ and $Cu(II)(NO_3)_2 \cdot 3H_2O$, both of which were purchased from Sigma-Aldrich, were used for the synthesis.

As reactants, glycerol from Alfa Aesar (+99%), acetol from Thermo Scientific (95%), 1,2-PDO from Sigma-Aldrich (99%), ethylene glycol from Roth (+98%), and methanol from Thermo Scientific (99.9%) were used. H_2 (5.0 grade, Linde) and N_2 (5.0 grade, Linde) were used for the catalytic experiments.

Catalyst Preparation

The powder catalyst was synthesized using a procedure based on Sherbi et al.'s[29] wetness impregnation method. The process mimics the procedure described in the literature, except that no calcination step was conducted, as shown in Figure 2.

The metal precursors were dissolved separately in a total of 820 mL of water and added to a round flask containing NANOCYL NC7000 carbon nanotubes, after which the pH of the solution was 2.5. The catalyst suspension was heated to 80 °C and stirred at 100 rpm by using a rotary evaporator for 5 h. After that, the water was removed using reduced pressure. The resulting powder was carefully mortared and dried in an oven (Nabertherm L9/11) for 8 h at 110 °C. Before use in a reaction, the catalyst was reduced in a tube furnace (Nabertherm R50/250/12) using forming gas with 5 vol % hydrogen in nitrogen at 550 °C for 8 h, with a heating rate of 120 °C h^{-1} and a gas flow of 50 L h^{-1}.

Subsequently, the catalyst was stored under an argon atmosphere inside a glass container until use.

Catalyst Characterization

The procedure for sample preparation is documented in the Supporting Information (section: sample digestion for ICP-OES).

https://doi.org/10.1021/acssuschemeng.6c02083
ACS Sustainable Chem. Eng. XXXX, XXX, XXX−XXX

The elemental concentrations of the following elements were determined by an inductively coupled plasma optical emission spectrometer (ICP-OES, PerkinElmer, Avio 550): Cu (327.393), Ru (240.272). To verify reproducibility and accuracy, individual sample splits were measured three times and compared against quality control standards with known concentrations. In most cases, the resulting blank values were found to be negligible; however, if a significant blank value was identified, then it was subtracted from the individual sample element concentrations.

Low temperature N_2 adsorption−desorption analysis was used (Nova 3000e Surface Area Analyzer, Quantachrome Instruments) to determine the mass specific surface area (S_m), mesopore size distribution, and mesopore volume (V_{meso}) of the catalysts. An overall sample mass of ≈ 20 mg was used for each analysis. Samples were degassed under a vacuum at a temperature of 100 °C for 6 h prior to analysis. S_m was estimated using the BET (Brunauer−Emmett−Teller) method based on highly correlated linear fitting of the BET model, p/p_0 range = 0.027−0.27, $R^2 \geq 0.9998$) derived from type IV N_2 adsorption isotherms. V_{meso} and the mean mesopore diameter ($d_{pore,\ mean}$) were estimated via the BJH (Barrett−Joyner−Halenda) method.

Batch Reactor Setup for Slurry Experiments

The experiments were conducted in a 300 mL stirred tank reactor (STR, Parr Instrument), equipped with a gas entrainment stirrer. The reactor, pipes, and valves were made of stainless steel (1.4571), and the gaskets were made of PTFE. A type K thermocouple with a stainless-steel sleeve, a heating mantle (Parr Instrument), and a thermostat (Peter Huber Kältemaschinenbau SE) were used to adjust the temperature. Gas was added manually via ball and needle valves. The pressure was controlled with an analog and digital pressure gauge. The reactor was connected to an online gas chromatograph (Bruker 450 GC) via heated tubes (200 °C) to prevent condensation of reactants and products, equipped with two flame ionization detectors (FID), one thermal conductivity detector (TCD), one methanizer, and four gas chromatography columns (Restek Q-Bond, Restek U-Bond, Bruker Swax, and Bruker Molsieve 5 Å) to analyze the gas composition. A scheme of the experimental setup is shown in Figure S1.

The liquid samples taken before, during, and after the reaction were analyzed by high-performance liquid chromatography (HPLC) for the detection of various products using a Nexera 40 (Shimadzu). For this purpose, each sample was filtered using syringe filters (0.45 μm) before analysis and measured using a polymer phase organic acid column (300 × 8 mm) from Chromatographie-Service GmbH. The measurements were conducted at 25 °C with a flow rate of 0.8 mL min^{-1} using an aqueous sulfuric acid solution with a concentration of 4 mmol L^{-1}. The signals were measured using a refractive index detector (RID). The detected products have been previously calibrated, as shown in the Supporting Information and Figure S2 (section: HPLC calibration).

Experimental Procedure

In a typical experiment, 1 g of the catalyst, along with water and the reactant, was prefed into the reactor. Of the total 300 mL reactor volume, 150 mL was filled with the reaction solution. After the reactor was closed, the stirrer speed was set to 300 rpm, and the reactor was purged once with 20 bar of nitrogen at room temperature to remove remaining air from the setup. Following this, the reactor was purged two more times with either 20 bar of hydrogen or nitrogen (depending on chosen reaction conditions). Next, the reactor was filled with hydrogen, nitrogen, or a mixture of the two gases to the desired initial pressure at room temperature. After leak tightness was ensured, the reaction temperature was set. After the desired temperature was reached, the reaction was started by setting the gas entrainment stirrer to 1000 rpm. Liquid samples for HPLC and gaseous samples for the online GC were taken at the start, end, and throughout the reaction. During the standard experiment, liquid samples were taken every 15 min for the first hour, then every 30 min for the second hour, and subsequently every hour thereafter until the experiment was terminated after a total of 7 h. GC samples were taken every 30 min for the first two hours and then every hour until the experiment was terminated. During the hydrogenation of acetol, liquid samples were taken every 5 min for the first 15 min and then every 15 min until the experiment was terminated after 90 min. GC samples were taken at the same time as the liquid samples whenever possible. However, due to long GC measurement times, it was only possible to analyze gas samples every 30 min.

Determination of the Kinetics and Calculations

The reaction rate was determined by plotting the concentrations of glycerol or the products against the reaction time. A linear fit was applied for the kinetic regime at low conversion, and the slope of the fit was taken as the reaction rate. The reaction order was determined by plotting the natural logarithm of the reaction rate against the initial concentrations of the reactants. Then, a linear fit was applied, and the slope was taken, giving the reaction order.

The following calculations were used to determine the reactant conversion (eq 1), product yield (eq 2), selectivity (eq 3), and overall carbon balance (eq 4):

$$X = \frac{c_{0,\mathrm{glycerol}} - c_{\mathrm{glycerol}}}{c_{0,\mathrm{glycerol}}} \times 100 \quad (1)$$

$$Y_i = \frac{c_i}{c_{0,\mathrm{glycerol}}} \times 100 \quad (2)$$

$$S_i = \frac{Y_i}{X} \times 100 \quad (3)$$

$$C_{\mathrm{balance}} = \frac{\sum n_i \times number\ of\ carbons}{n_{0,\mathrm{glycerol}} \times 3} \times 100 \quad (4)$$

The Arrhenius plot was used to determine the activation energy from the temperature variation experiments. The Arrhenius plot is derived from the Arrhenius eq (eq 5) by applying a natural logarithm (eq 6).

$$k = A \cdot e^{-E_a/RT} \quad (5)$$

$$\ln(k) = \ln(A) - \frac{E_a}{R} \cdot \frac{1}{T} \quad (6)$$

RESULTS AND DISCUSSION

Catalyst Characterization

ICP analysis of the synthesized Ru−Cu/CNT catalyst was conducted to verify that the desired metal loading was achieved, as shown in Table 1. The ICP results indicate that the actual metal weight of the catalyst is close to the theoretical weight, and the desired catalyst loading of 5% was successfully achieved.

Table 1. ICP Results of the Synthesized Catalyst

catalyst	theoretical Wt. (g kg^{-1})	ICP-OES Wt. (g kg^{-1})	ICP-OES loading (%)
$RuCu_2$@ NC7000	Ru: 22.1 Cu: 27.9	Ru: 20.7 Cu: 28.8	4.95

Table 2 summarizes the textural properties of the synthesized bimetallic catalyst. The catalyst exhibits a type IVa isotherm, as expected for a mesoporous material (pore size distribution has a maximum at around 30−50 nm). Compared to pure CNTs, the total surface area decreases after metal impregnation. This decrease can be attributed to metal particles either being deposited within the pores or blocking their entrances. However, the total pore volume increased upon metal loading, suggesting that the metals were primarily

https://doi.org/10.1021/acssuschemeng.6c02083
ACS Sustainable Chem. Eng. XXXX, XXX, XXX−XXX

Table 2. Physico-Chemical Properties of the Synthesized Catalyst

catalyst/support	[a]total surface area (m^2 g^{-1})	[b]pore volume (cc/g)	[b]pore diameter (nm)	[c]Metal dispersion (%)	[c]particle diameter (nm)	[c]particle diameter after reduction/nm
NC7000	252	0.919	14.8	—	—	—
$RuCu_2$/NC7000	205 ± 2	1.155	22.6	72.50	1.14 ± 0.21	1.83 ± 0.43

[a]Determined with N_2-physisorption using the BET method. [b]Determined with N_2-physisorption using the BJH method. [c]Determined with HR-TEM.

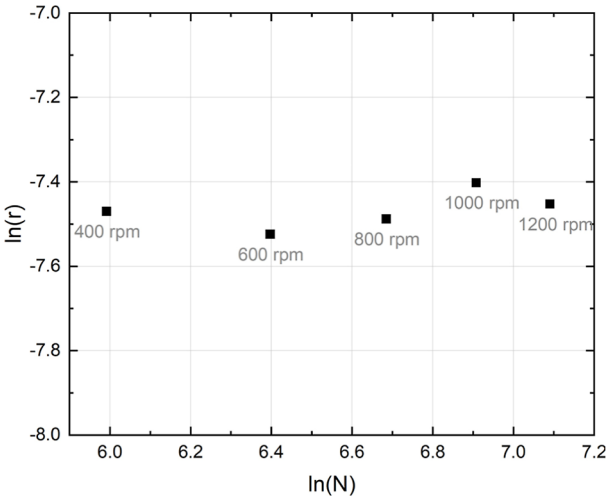

Figure 3. Logarithmic reaction rate (r) of glycerol hydrogenolysis at different stirrer speeds (N). Reaction conditions: V = 150 mL, T = 220 °C, $p_0(H_2)$ = 20 bar, p(total) = 50 bar, t = 7 h, $c_{Glycerol}$ = 20 wt %, $m_{catalyst}$ = 1 g, and solvent: H_2O.

deposited on the outer surface of the CNTs, possibly near the pore openings. This could lead to an extension of the accessible pore system, thereby increasing its volume. Additionally, the average pore diameter was found to be slightly larger in the bimetallic catalyst compared to that in pure CNTs. This may indicate that smaller pores are more likely to be blocked by metal particles, rendering them inaccessible and shifting the average diameter toward larger values. In contrast, wider pores are less likely to be completely blocked, which helps to explain the observed increase in pore volume.

Influence of Catalyst Loading

The amount of the catalyst used was varied between 200 and 1000 mg to observe the effect of catalyst loading on the reaction rate, which is shown in Figure S3. The reaction rate increased linearly with catalyst loading, giving a slope of 0.82 and an R^2 of 0.91. For the following experiments, a catalyst loading of 1000 mg was chosen to achieve maximum reaction rates. A blank experiment without any catalyst was conducted and showed no glycerol conversion (Figure S4).

Investigations on Heat and Mass Transfer Limitations

Understanding the reaction mechanism and determining intrinsic kinetic parameters require exclusion of potential heat and mass transfer limitations. However, the kinetics of glycerol hydrogenolysis can only be accurately determined if external factors, such as mass and heat transport, do not affect the observed reaction rate.

Therefore, we investigated the potential mass transport limitations by varying the stirrer speed from 400 up to 1200 rpm at a reaction temperature of 220 °C (see Figure 3). Twenty bar of hydrogen pressure were chosen due to the fact that the reaction is more likely to be mass transport-limited at low hydrogen pressures, according to Fick's law stating that the rate of diffusion is directly dependent on the concentration gradient, which is slower for lower hydrogen pressures.[44] The linearized reaction rates show that the latter does not increase with an increasing stirring speed. Therefore, the reaction is not film diffusion-limited under the applied reaction conditions. For the following experiments, a stirring speed of 1000 rpm was chosen to guarantee the maximum gas entrainment.

In a stirred tank reactor using water as the solvent, no heat transfer limitations are expected. This is due to water's high specific heat capacity, which enables efficient heat absorption and dissipation. Additionally, continuous stirring ensures a homogeneous temperature distribution in the reactor, minimizing temperature gradients. These properties ensure effective heat transfer, thereby preventing the occurrence of heat transfer limitations.

Since the reaction is not mass transfer-limited and potential heat transfer limitations can be disregarded under the applied reaction conditions, the observed kinetics (r_{eff}) are equal to the intrinsic kinetics (r_{int}) of the reaction. The kinetics can be calculated using eq 7. The integrated rate law was chosen since the experiment was conducted in a STR, wherein the reactant concentration, catalyst distribution, and reaction temperature were assumed to be homogeneous throughout the liquid phase.

$$r_{eff} = k_{eff} \cdot c_{Gly}^{a} \cdot c_{H_2}^{b} = r_{int} = k_{int} \cdot c_{Gly}^{a} \cdot c_{H_2}^{b} \quad (7)$$

Reactants' Influence on the Kinetics

To investigate the influence of the glycerol concentration on the reaction rate, the initial glycerol concentration was varied between 2.5 and 80 wt % according to the literature.[31−35] Figure 4 shows the temporal profiles for the various initial glycerol concentrations with the corresponding fits and conversion−time graphs. The initial glycerol concentrations are shown in Table S1. Reproducibility studies carried out at 25 bar H_2 pressure (Figure S7) confirmed the standard deviation for the conversion of 1.09%, 2.29% for the 1,2-PDO yield, and 2.18% for the 1,2-PDO selectivity, as well as 1.56% for the carbon balance.

Glycerol is consumed during the reaction, and a higher glycerol concentration leads to a higher conversion rate. Therefore, the reaction rate for glycerol increases with an increase in the initial glycerol concentration. However, it does not increase to the same degree as the concentration. The reaction order for glycerol can be determined using the natural logarithm of eq 5, shown in eq 8, and plotting the $\ln(r_{int})$ value determined through the linear regression shown in Figure 4 against $\ln(c_{Gly,0})$.

$$\ln(r_{int}) = \ln(k) + a \cdot \ln(c_{glycerol,0}) \quad (8)$$

Figure 5a plots the natural logarithm of the reaction rates against the initial glycerol concentrations. As the initial glycerol concentration increases, so does the reaction rate. The reaction order with respect to the glycerol concentration was 0.66.

https://doi.org/10.1021/acssuschemeng.6c02083
ACS Sustainable Chem. Eng. XXXX, XXX, XXX−XXX

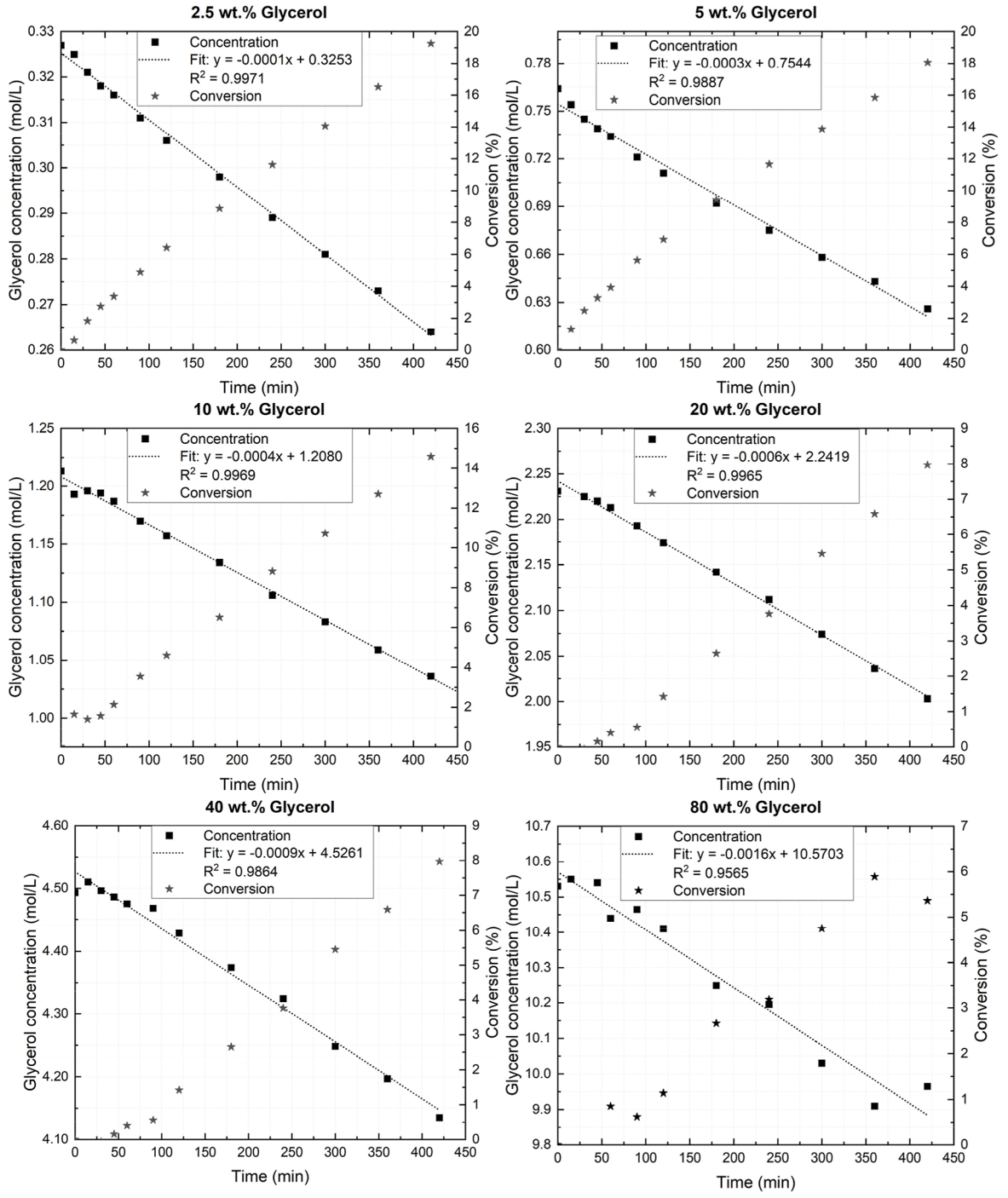

Figure 4. Temporal profiles of the glycerol concentration and conversion at varying initial glycerol concentrations. Reaction conditions: V = 150 mL, T = 220 °C, $p_0(H_2)$ = 50 bar, t = 7 h, $m_{catalyst}$ = 1 g, and solvent: H_2O. $N_{stirrer}$ = 1000 rpm.

Figure 5b shows the same data but just for the formation of the products along the desired 1,2-PDO pathway. The products include acetol, 1,2-PDO, and n-propanol, as shown in Figure 1. Ethanol is also included, as stability experiments in this study showed that ethanol is derived from 1,2-PDO rather than from ethylene glycol under the applied reaction conditions (Figure 13). A table of the starting and final pathway concentrations is provided in Table S2. A reaction order of 1.17 was determined with respect to the initial glycerol concentration. This matches first-order values reported for other Cu-based catalysts in the literature.[33,34] The reaction order for the products resulting from the ethylene glycol pathway is shown in Figure S5 and is 0 with respect to that of glycerol. Notably, all products that could not be identified were included in this pathway for simplification.

Figure 6 illustrates the glycerol conversion (X), 1,2-PDO yield (Y) and selectivity (S) after 7 h reaction time for various initial glycerol concentrations. The corresponding temporal 1,2-PDO yield is shown in Figure S6. As the glycerol concentration increases, the conversion rate decreases from 19.2% (2.5 wt %) to 5.4% (80 wt %), while the selectivity increases from 12.7 to 84.9%. However, the 1,2-PDO yield shows a maximum of 8.6% at 10 wt % glycerol. The decrease in conversion indicates that an increase in the reaction rate does

https://doi.org/10.1021/acssuschemeng.6c02083
ACS Sustainable Chem. Eng. XXXX, XXX, XXX−XXX

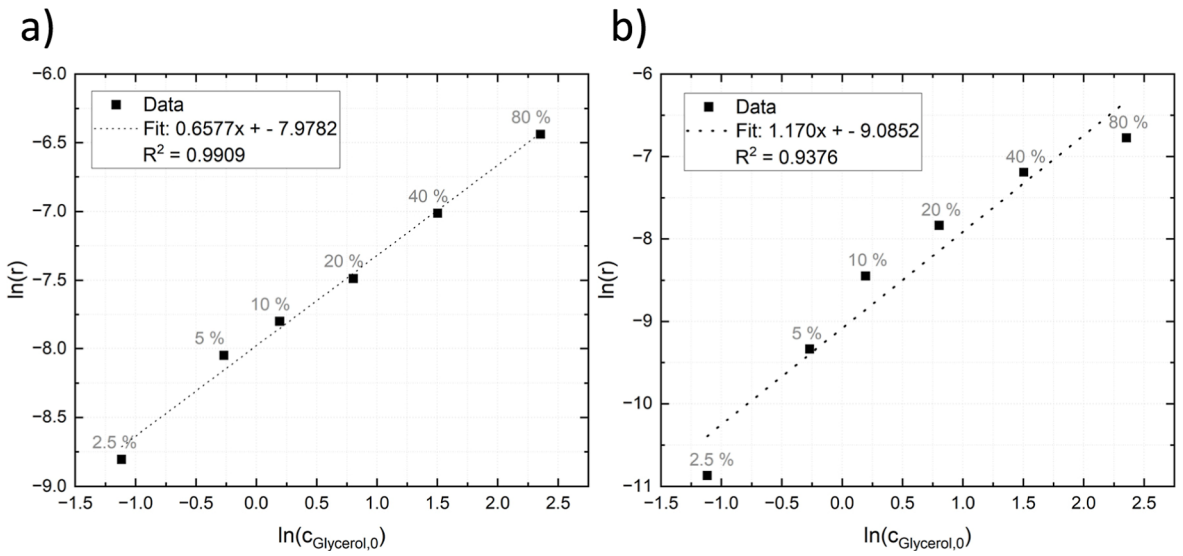

Figure 5. Graphical determination of the reaction order for (a) glycerol consumption and (b) 1,2-PDO pathway products by variation of the initial glycerol concentration. Reaction conditions: V = 150 mL, T = 220 °C, $p_0(H_2)$ = 50 bar, t = 7 h, $m_{catalyst}$ = 1 g, and solvent: H_2O. $N_{stirrer}$ = 1000 rpm.

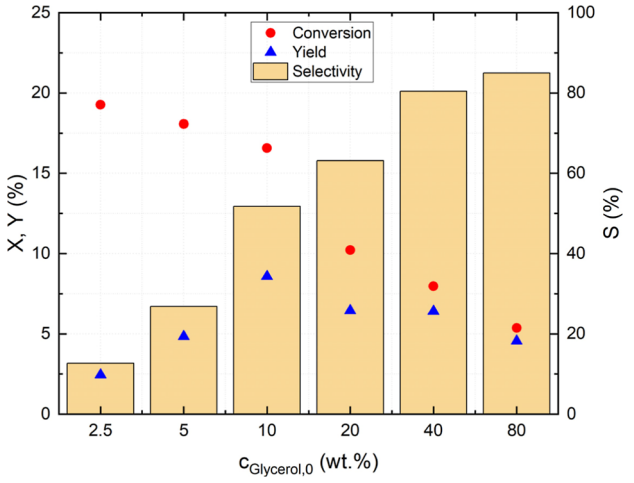

Figure 6. Overview on glycerol conversion (X), yield (Y), and selectivity (S) of 1,2-PDO at the end of the experiment for varying initial glycerol concentrations. Reaction conditions: V = 150 mL, T = 220 °C, $p_0(H_2)$ = 50 bar, t = 7 h, $N_{stirrer}$ = 1000 rpm, $m_{catalyst}$ = 1 g, and solvent: H_2O.

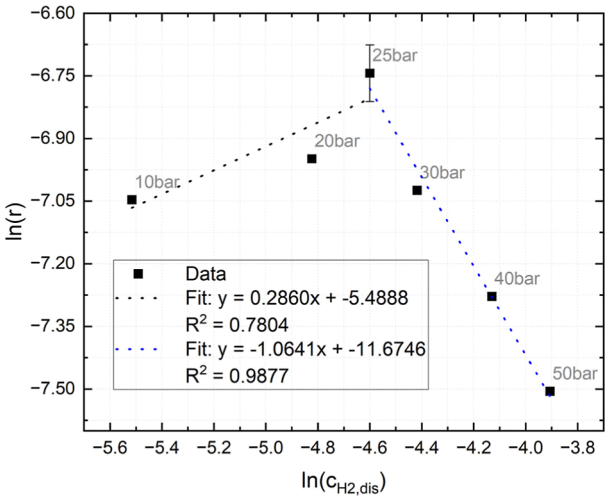

Figure 7. Graphical determination of the reaction order for the glycerol consumption for different initial hydrogen concentrations. Reaction conditions: V = 150 mL, T = 220 °C, t = 7 h, $N_{stirrer}$ = 1000 rpm, $c_{Glycerol}$ = 20 wt %, $m_{catalyst}$ = 1 g, and solvent: H_2O. The experiment at a hydrogen pressure of 25 bar was conducted three times giving a standard deviation of + −1.09 (Figure S7).

not necessarily result in higher glycerol conversion. The opposite is true: Conversion decreases with an increased initial glycerol concentration. This occurs because the reaction rate increases more slowly compared with the increasing glycerol concentration, as stated above.

With the increasing initial glycerol concentration, the reaction becomes gradually more selective for 1,2-PDO. The 1,2-PDO yield, however, reaches a maximum at 10 wt % glycerol and then begins to decrease due to the reduced conversion. For the following set of experiments, 20 wt % initial glycerol concentration was chosen, as it strikes a good balance between activity and selectivity.

To determine the reaction order for the gaseous reactant hydrogen, the initial hydrogen partial pressure was varied from 10 to 50 bar while maintaining a total system pressure of 50 bar using nitrogen for balancing. The concentration of dissolved hydrogen in the liquid phase was calculated using Henry's law, as shown in eq 9.[45]

$$c_{H_2,dis} = H_s^{cp} \cdot p_{H,2} \quad (9)$$

The reaction rate and order are strongly dependent on the concentration of dissolved hydrogen, as shown in Figure 7.

Each glycerol concentration over time plot for the different initial hydrogen pressures is shown in Figure S7. At low hydrogen pressures up to 25 bar and therefore at low dissolved hydrogen concentrations, the reaction rate increases with higher H_2 pressure, exhibiting a reaction order of 0.29. At 25 bar, the maximum reaction rate was reached. From 25 to 50 bar, the reaction rate decreases sharply, exhibiting a negative reaction order of −1.06.

At low hydrogen pressures, the reaction is kinetically limited; thus, increasing the hydrogen pressure increases the reaction rate up to a maximum at 25 bar. A possible explanation for the decreasing reaction rate at increased hydrogen pressures (>25 bar) could be the increasing saturation of the catalyst surface

https://doi.org/10.1021/acssuschemeng.6c02083
ACS Sustainable Chem. Eng. XXXX, XXX, XXX−XXX

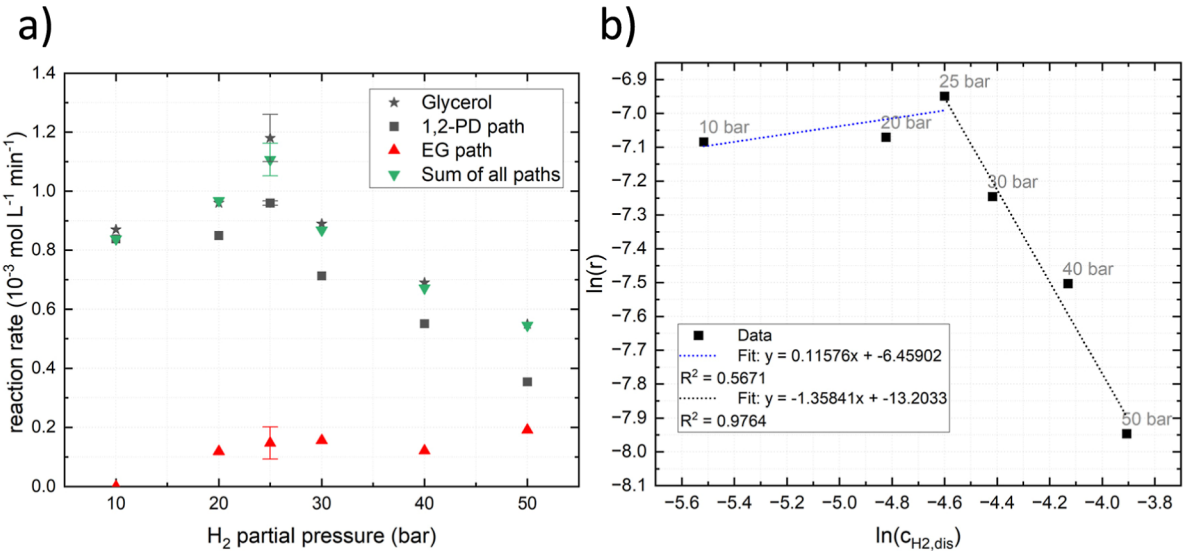

Figure 8. (a) Reaction rates at different initial hydrogen pressures regarding different reactants and products. (b) Graphical determination of the reaction order for 1,2-PDO pathway production for different initial hydrogen concentrations. Reaction conditions: V = 150 mL, T = 220 °C, t = 7 h, $N_{stirrer}$ = 1000 rpm, $c_{0,Glycerol}$ = 20 wt %, $m_{catalyst}$ = 1 g, and solvent: H_2O. The experiment at a hydrogen pressure of 25 bar was conducted three times (Figure S7).

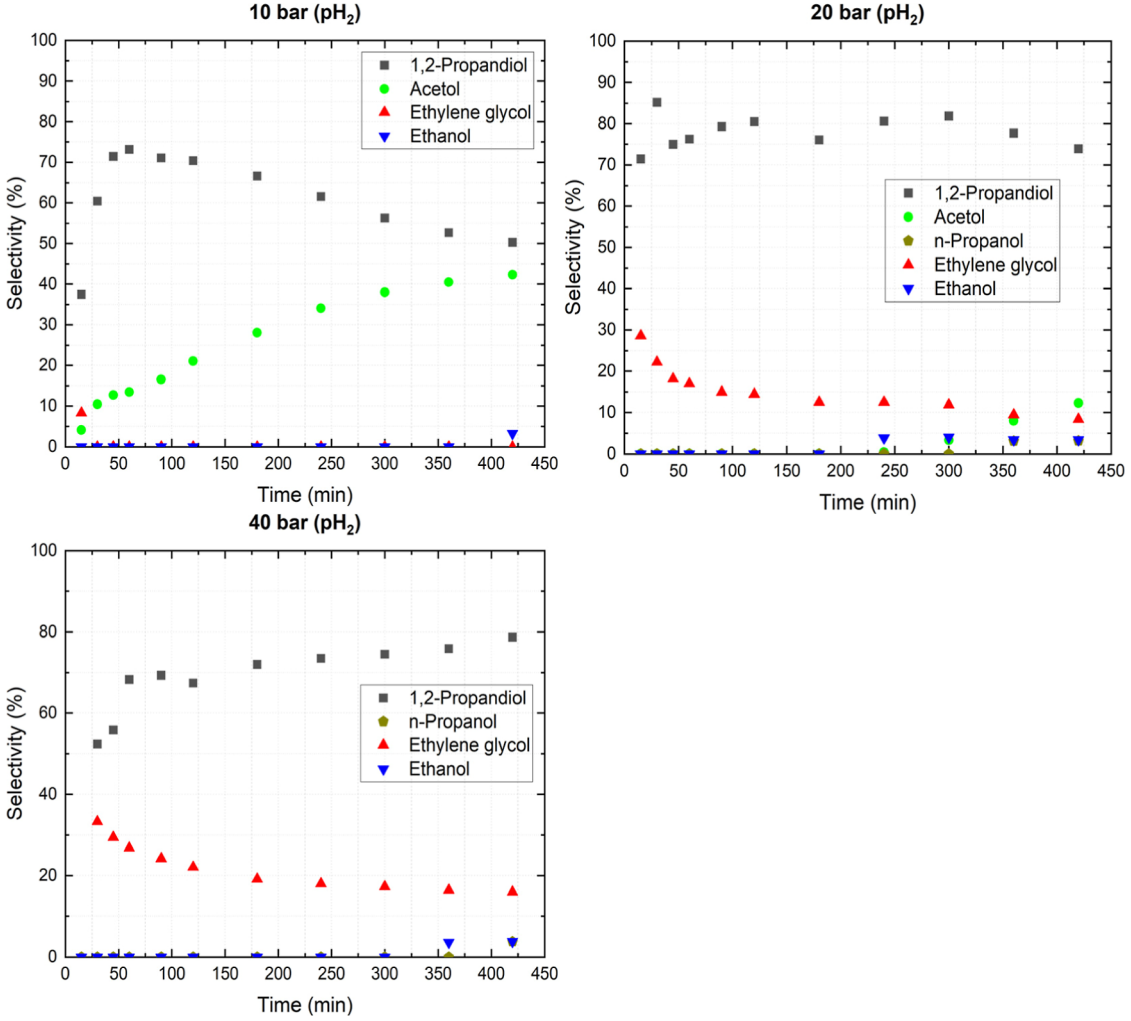

Figure 9. Temporal selectivity profiles for different initial hydrogen pressures. Reaction conditions: V = 150 mL, T = 220 °C, t = 7 h, $N_{stirrer}$ = 1000 rpm, $c_{0,Glycerol}$ = 20 wt %, $m_{catalyst}$ = 1 g, and solvent: H_2O.

https://doi.org/10.1021/acssuschemeng.6c02083
ACS Sustainable Chem. Eng. XXXX, XXX, XXX−XXX

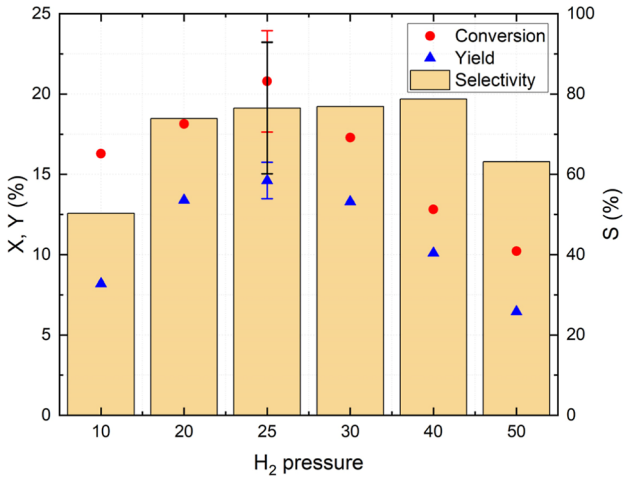

Figure 10. Overview of glycerol conversion (X), yield (Y), and selectivity (S) of 1,2-PDO at different initial hydrogen pressures at the end of the kinetic experiments. Reaction conditions: V = 150 mL, T = 220 °C, t = 7 h, $N_{stirrer}$ = 1000 rpm, $c_{0,glycerol}$ = 20 wt %, $m_{catalyst}$ = 1 g, and solvent: H_2O. The experiment at a hydrogen pressure of 25 bar was conducted three times.

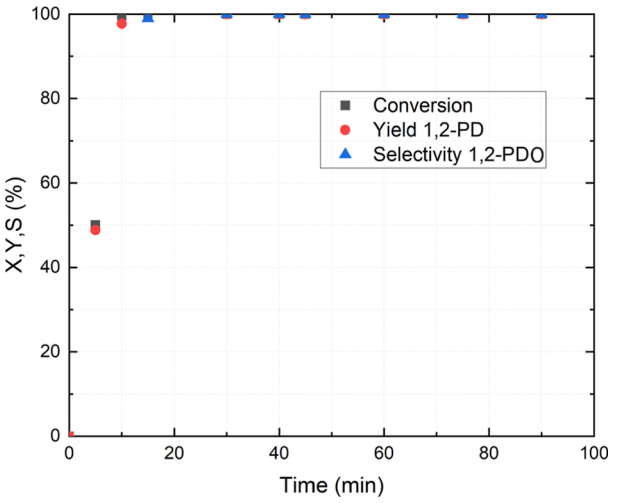

Figure 12. Conversion (X), yield (Y), and selectivity (S) for the acetol hydrogenation to 1,2-PDO. Reaction conditions: V = 150 mL, T = 145 °C, $p_0(H_2)$ = 25 bar, t = 100 min, $N_{stirrer}$ = 1000 rpm, $c_{0,Acetol}$ = 5 wt %, $m_{catalyst}$ = 1 g, and solvent: H_2O.

with hydrogen, blocking the further adsorption of the bigger glycerol molecules.

The kinetics of the individual reaction pathways were further studied to determine their reaction rates and their influence on the kinetics of the overall hydrogenolysis reaction. Since both the C−C cleavage leads to ethylene glycol and methanol and the desired C−O cleavage leads to 1,2-PDO consume glycerol, the corresponding reaction rates cannot be determined separately from the glycerol conversion curves. Figure 8a illustrates the reaction rates of the two pathways at different initial hydrogen pressures. It also includes the overall reaction rate, based on the glycerol consumption, as well as the sum of the reaction rates of the individual paths. The sum of all paths is determined by adding the reaction rates of both the 1,2-PDO and the EG pathways.

Figure 8a illustrates that the 1,2-PDO pathway is the dominating pathway in the overall reaction. A table of the starting and final pathway concentrations is provided in the Supporting Information (Table S3). At initial hydrogen pressures of 10 and 20 bar, the reaction rate for the 1,2-PDO pathway remains constant and then increases to a maximum at 25 bar. The reaction rate then decreases with increasing initial hydrogen pressure, similar to the reaction rate determined by the glycerol concentration. Analogous to the previous results, this suggests a kinetic limitation at low hydrogen pressures and a limitation through reactant adsorption at high hydrogen pressures.

The reaction rate for the EG pathway is zero at 10 bar, and the reaction rate for 1,2-PDO matches the reaction rate derived from glycerol. At pressures of 20 bar and higher, the reaction rate of the EG pathway remains constant.

The sum of the individual reaction rates matches the overall reaction rate derived from the temporal glycerol concentration. This shows that separating the reaction rates is a suitable method for investigating the kinetics of the individual pathways.

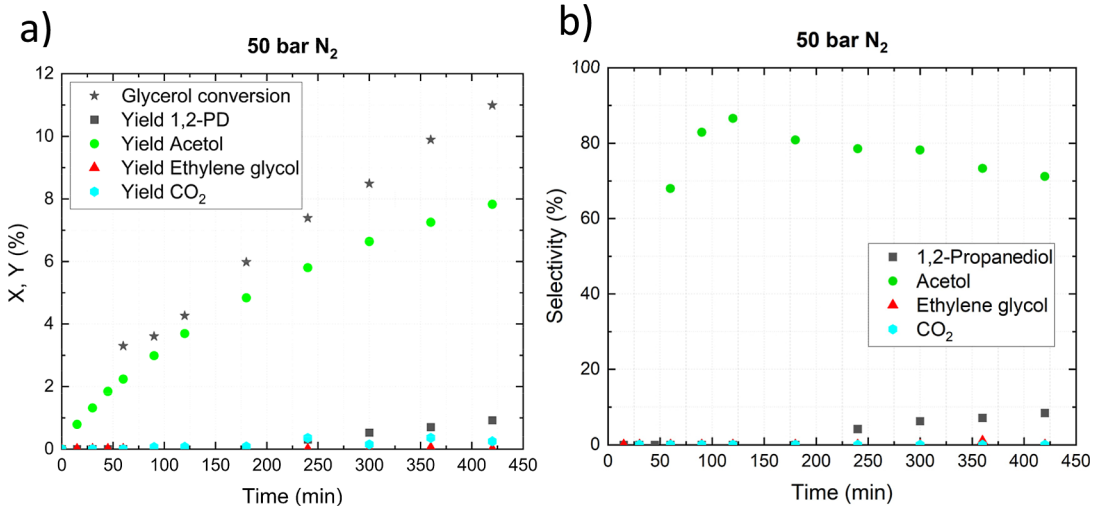

Figure 11. (a) Conversion (X) and 1,2-PDO yield (Y) and (b) 1,2-PDO selectivity (S) for the dehydration of glycerol under 50 bar nitrogen pressure. Reaction conditions: V = 150 mL, T = 220 °C, t = 7 h, $N_{stirrer}$ = 1000 rpm, $c_{0,Glycerol}$ = 20 wt %, $m_{catalyst}$ = 1 g, and solvent: H_2O.

https://doi.org/10.1021/acssuschemeng.6c02083
ACS Sustainable Chem. Eng. XXXX, XXX, XXX−XXX

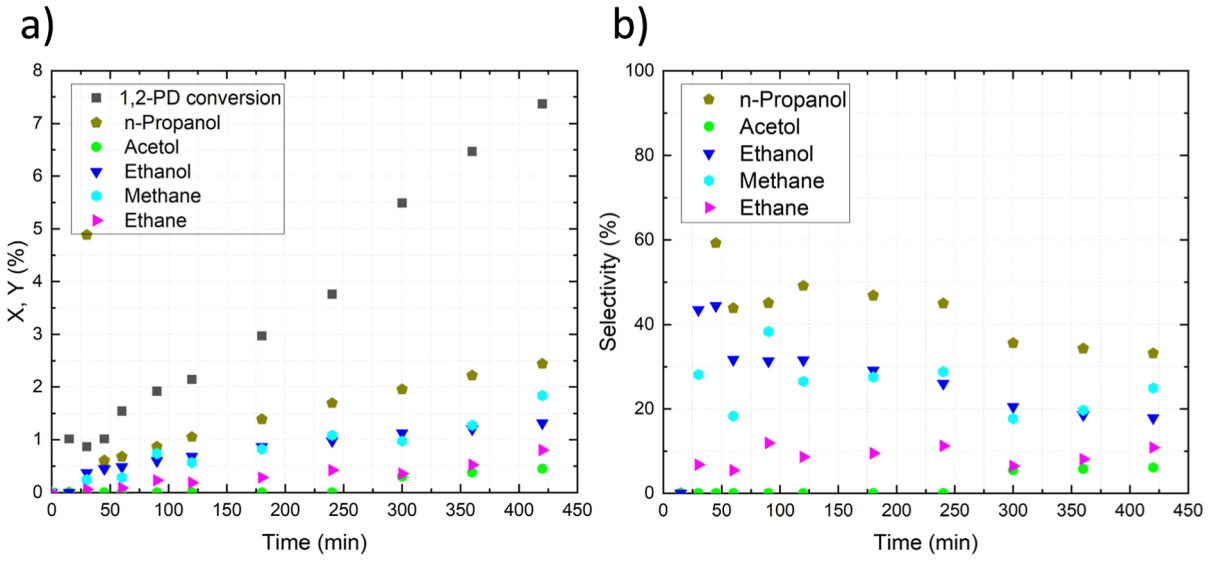

Figure 13. 1,2-PDO stability over time under typical hydrogenolysis conditions. (a) 1,2-PDO conversion and product yields and (b) product selectivities. Reaction conditions: V = 150 mL, T = 220 °C, $p_0(H_2)$ = 25 bar, t = 7 h, $N_{stirrer}$ = 1000 rpm, $C_{o,1,2\text{-PDO}}$ = 20 wt %, $m_{catalyst}$ = 1 g, and solvent: H_2O.

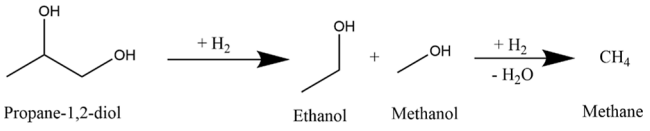

Figure 14. Proposed decomposition route of 1,2-PDO to ethanol and methanol and further to methane under typical hydrogenolysis conditions.

Figure 8b shows the graphical determination of the reaction order for the 1,2-PDO pathway-derived products regarding hydrogen. At 10 to 25 bar hydrogen pressure, a reaction order of 0.12 was determined. At higher pressures, a reaction order of −1.36 with respect to hydrogen was found. The reaction order for ethylene glycol pathway-derived products was found to be zero and is shown in the Supporting Information (Figure S8).

As discussed above, the diverse reaction pathways were affected differently by the change in the initial hydrogen pressure. This was proven through HPLC and GC analytics, as shown by the temporal selectivity profiles in Figure 9.

At 10 bar initial hydrogen pressure, the selectivity for 1,2-PDO increases up to 73.1% until 60 min reaction time and then decreases over time to 50.3%, after 420 min, while the selectivity for the key intermediate acetol increases throughout the reaction to 42.3%. In addition, no ethylene glycol is formed. The decreasing 1,2-PDO selectivity suggests that the reaction becomes limited by hydrogen availability with a progressing reaction. At higher conversion, not enough hydrogen is available to fully hydrogenate the acetol formed from the initial dehydration and keto−enol tautomerization, resulting in an increase in selectivity for the intermediate acetol. However, the C−C-cleavage to ethylene glycol could be entirely avoided. Therefore, under low hydrogen pressures, the reaction is very selective for the desired 1,2-PDO pathway. In addition, since no ethylene glycol is formed, the reaction rate of the 1,2-PDO path is the same as the reaction rate determined through the glycerol concentration. This matches the results observed in Figure 8.

At 20 bar initial hydrogen pressure, the 1,2-PDO selectivity increases slightly until reaching a maximum at 120 min of 80.5%, then remains constant until 360 min and then starts to decline to 73.9%. Simultaneously, at 360 min, the acetol selectivity starts to increase from 3.3% to a maximum of 12.3% at the end of the reaction. This suggests that the reaction remains hydrogen-limited but only at high conversion rates. In contrast to the 10 bar experiment, ethylene glycol is formed, and the selectivity starts from 25.6% after preheating and then decreases over time to 8.4%. Furthermore, ethanol is formed after 180 min resulting from consecutive decomposition of ethylene glycol.

At 40 bar of initial hydrogen pressure, the selectivity curves resemble the 20 bar curves at first glance. However, the 1,2-PDO curve does not decrease at later reaction times; instead, it increases until the end of the reaction to a final selectivity of 78.7%. Additionally, there is no detectable acetol formation, and the final selectivity for ethylene glycol of 16.0% is higher compared to the 20 bar experiment. The absence of acetol formation suggests that there is enough hydrogen available to immediately hydrogenate all available acetol and that acetol hydrogenation which is significantly faster than glycerol dehydration. Additionally, ethylene glycol formation appears to increase relative to 1,2-PDO formation. This relative increase occurs because the reaction rate for the 1,2-PDO pathway decreases with a higher hydrogen pressure, while the reaction rate for ethylene glycol formation remains constant, as previously shown in Figure 8.

Figure 10 presents an overview of the end point values for glycerol conversion, yield, and selectivity of 1,2-PDO determined after 420 min reaction time for different initial hydrogen pressures. The corresponding temporal conversion and yield plots are shown in Figures S7 and S8.

The results show that there is not only a kinetic maximum of the overall reaction rate at 25 bar of initial hydrogen pressure as illustrated in Figure 7 but also the highest glycerol conversion (20.8%) and the highest 1,2-PDO yield (14.6%) at an excellent 1,2-PDO selectivity (76.5%) were achieved here. This holds, even though a high deviation was observed between the experiments for glycerol conversion values (which influenced the selectivity values), indicating that 25 bar is the

https://doi.org/10.1021/acssuschemeng.6c02083
ACS Sustainable Chem. Eng. XXXX, XXX, XXX−XXX

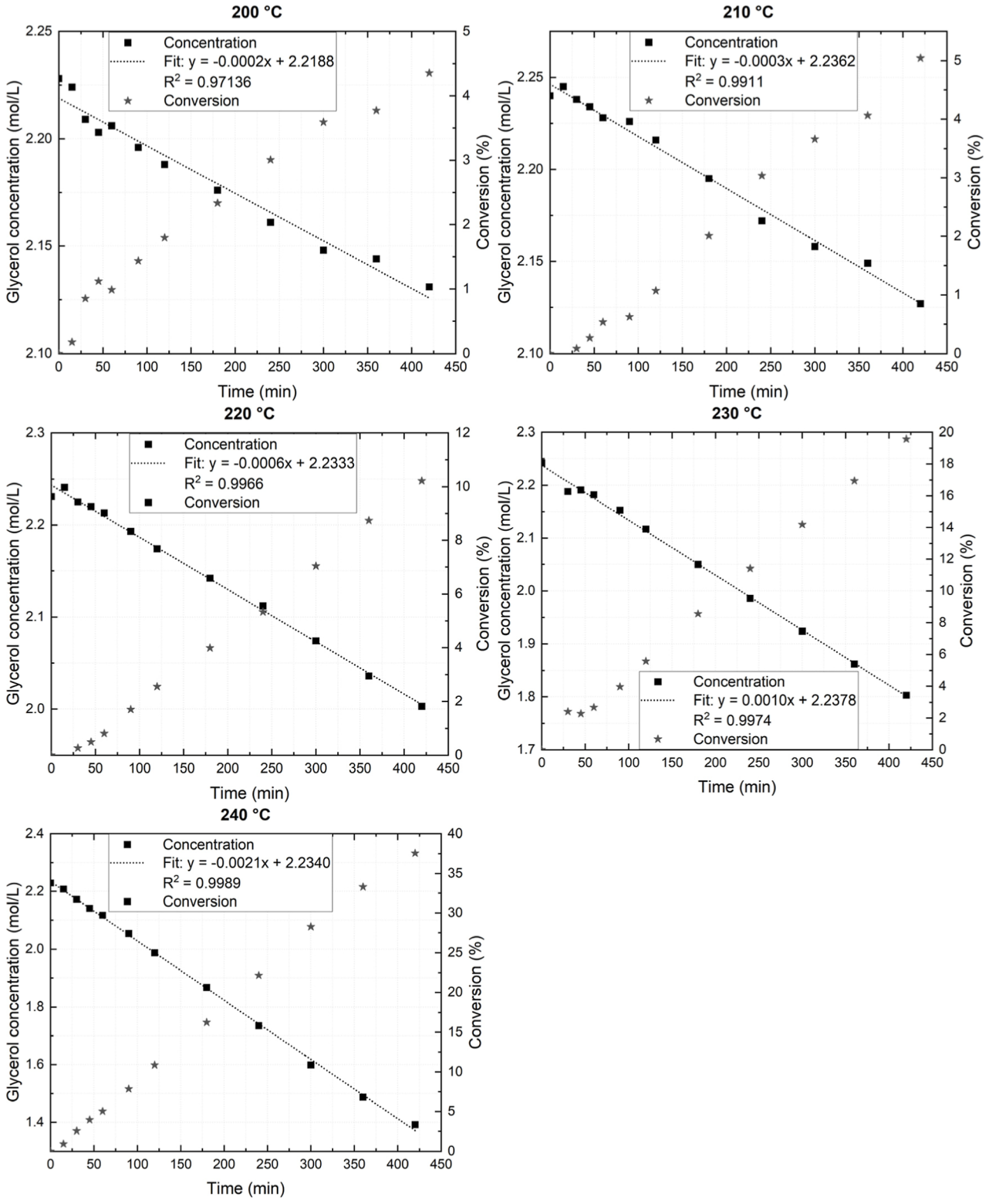

Figure 15. Temporal profiles of the glycerol concentration and conversion at varying reaction temperatures. Reaction conditions: V = 150 mL, $p_0(H_2)$ = 50 bar, t = 7 h, $N_{stirrer}$ = 1000 rpm, $c_{0,Glycerol}$ = 20 wt %, $m_{catalyst}$ = 1 g, and solvent: H_2O.

optimal initial hydrogen pressure for glycerol hydrogenolysis to 1,2-PDO.

Glycerol Dehydration

In the next set of experiments, we tried to separate the individual reaction steps in order to verify whether the used RuCu/CNT catalyst prefers one of the individual steps. As the individual subreactions cannot be isolated under typical hydrogenolysis conditions, we had to adopt the reaction conditions in order to allow for a separate investigation of the individual steps. Therefore, to investigate solely the glycerol dehydration and subsequent keto−enol tautomerization to acetol, this set of experiments was conducted under a pure

https://doi.org/10.1021/acssuschemeng.6c02083
ACS Sustainable Chem. Eng. XXXX, XXX, XXX−XXX

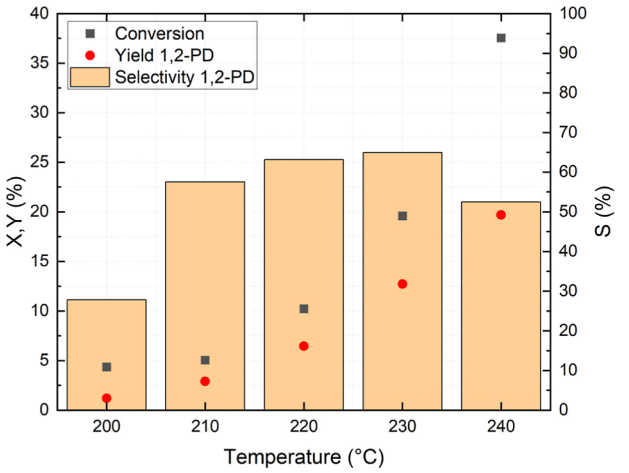

Figure 16. Overview of glycerol conversion (X), yield (Y), and selectivity (S) of 1,2-PDO at different reaction temperatures. Reaction conditions: V = 150 mL, $p_0(H_2)$ = 50 bar, t = 7 h, $N_{stirrer}$ = 1000 rpm, $c_{0,glycerol}$ = 20 wt %, $m_{catalyst}$ = 1 g, and solvent: H_2O.

nitrogen atmosphere of 50 bar to prevent consecutive hydrogenation to 1,2-PDO, as previously suggested by Chiu et al.[36] The temporal plots for conversion (X), 1,2-PDO yield (Y), and 1,2-PDO selectivity (S) for acetol are shown in Figure 11.

The observed glycerol conversion starts slowly with a value of 3.3% after 60 min reaction time and continues to increase over time, reaching a maximum of 11% by the end of the experiment after 420 min. The acetol yield constantly increases during the reaction, first rapidly up to 120 min and then gradually to 7.8% after 420 min. Corresponding to the slowdown in acetol yield, the yield of 1,2-PDO increases during the second half of the experiment to 0.9%. Moreover, also traces of CO_2 could be detected in the gas phase resulting from decarboxylation. As anticipated, dehydration indeed occurs in the absence of hydrogen, as evidenced by the formation of acetol during the reaction. The small presence of 1,2-PDO at higher conversions was not unexpected, as Chiu et al.[36] already reported observing 1,2-PDO formation during the glycerol dehydration under the exclusion of external hydrogen.

Table 3. Kinetic Parameters as Estimated by the Kinetic Model

parameter	Kinetic model	confidence intervals	experimentally determined
$k_{0,1}(M^{(1-n)}/\text{min})$	4.13×10^9	$[1.2 \times 10^8, 1.4 \times 10^{11}]$	1.60×10^{10}
$E_{A,1}$(KJ/mol)	149	[136, 165]	154
$n_{Gly,1}(-)$	1.04	[1.00, 1.07	1.17
$n_{H,1}/-$	−1.31	[-1.40, −1.21]	−1.36
$k_{0,2}/M^{(1-n)}/\text{min}$	4.85×10^3	$[1.08 \times 10^2, 2.18 \times 10^5]$	4.92×10^2
$E_{A,2}$/KJ/mol	69	[56, 86]	60
$n_{Gly,2}(-)$	0.06	[-0.006, 0.116]	0
$n_{H,2}/-$	0.00	[-0.179, 0.175]	0

They postulated that the formation of 1,2-PDO is due to the scavenging of hydrogen from glycerol. A different explanation could be the reforming of glycerol to hydrogen and CO_2 catalyzed by the Ru catalyst as suggested by Roy et al.[46]

The final conversion rates of 10.2% at 50 bar hydrogen pressure (see Figure 10) and 11% at 50 bar nitrogen pressure (Figure 11) resemble each other. This suggests that dehydration to acetol is the rate-determining step in the overall hydrogenolysis reaction. However, the final acetol yield of 7.8% for glycerol dehydration is higher compared to the 1,2-PDO yield of 6.0% for the analogues hydrogenolysis experiment. The increased yield is due to the lack of hydrogen, which completely suppresses ethylene glycol formation, thereby increasing the dehydration to acetol. In addition, a higher selectivity of 71.2% for acetol was achieved (79.6% if 1,2-PDO is included) compared to the 63% selectivity of 1,2-PDO during the hydrogenolysis, also due to the suppression of ethylene glycol formation.

Acetol Hydrogenation

To study the hydrogenation of acetol to 1,2-PDO separately, acetol was used as the reactant instead of glycerol for the next set of experiments. Kinetic measurements for acetol hydrogenation were not possible at 220 °C because the reaction occurred so quickly that all reactants would already be consumed during the heating-up phase. Therefore, an

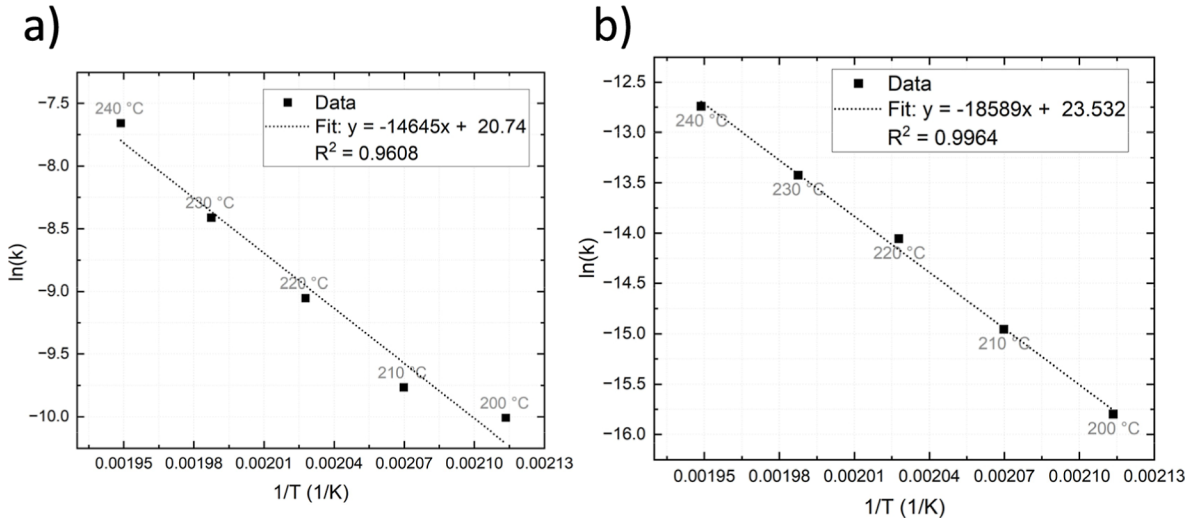

Figure 17. Arrhenius plot to determine the activation energy for (a) the glycerol consumption and (b) the 1,2-PDO pathway products. Reaction conditions: V = 150 mL, $p_0(H_2)$ = 50 bar, t = 7 h, $N_{stirrer}$ = 1000 rpm, $c_{0,glycerol}$ = 20 wt %, $m_{catalyst}$ = 1 g, and solvent: H_2O.

https://doi.org/10.1021/acssuschemeng.6c02083
ACS Sustainable Chem. Eng. XXXX, XXX, XXX−XXX

additional series of temperature variation experiments was conducted to identify the optimum temperature to study the kinetics of acetol hydrogenation. Reducing the reaction temperature to 145 °C allowed for the determination of kinetic parameters with the current reaction setup. To ensure that not all hydrogen would be consumed and subsequently acetol would remain non-hydrogenated, the acetol loading was set to 5 wt %. Figure 12 shows the temporal acetol conversion (X), 1,2-PDO-yield (Y), and 1,2-PDO-selectivity (S) for the acetol hydrogenation experiments. Both conversion and yield increase rapidly at the start of the experiment, reaching already 99% after 10 min and 100% after 15 min. This shows that hydrogenating acetol to 1,2-PDO is significantly faster than dehydrating glycerol to acetol, even at lower temperatures. In addition, the rate of acetol hydrogenation indicates that acetol is only present at low hydrogen pressures because not all of the acetol can be fully hydrogenated due to lack of hydrogen. The selectivity curve is between 99% and 100% due to the fact that all of the consumed acetol is only hydrogenated to 1,2-PDO.

Furthermore, no undesired hydrogenolysis of 1,2-PDO to n-propanol, which was observed at higher reaction temperatures of 220 °C for the overall reaction, could be observed, showing the potential of gaining nearly perfect selectivity when separating both reaction steps using the multifunctional Ru−Cu/CNT catalyst. To investigate whether hydrogenation remains selective in the presence of glycerol, a hydrogenation experiment using a reaction solution containing 7.5 wt % glycerol and acetol was conducted. As shown in Figure S11, acetol is completely hydrogenated to 1,2-PDO, while glycerol is not converted at all.

Product Stability

To investigate the potential decomposition of the C−C-cleavage products ethylene glycol and methanol under typical hydrogenolysis conditions of 220 °C and 25 bar hydrogen pressure using the Ru−Cu/CNT catalyst, a 20 wt % solution of equal molar amounts of ethylene glycol and methanol was used as a reactant. Under these conditions, ethylene glycol remained stable, while approximately 11% methanol decomposed into methane (see Figure S12). Interestingly, ethylene glycol did not decompose to ethanol, which was found as a product in other experiments (see Figure 9), indicating that a different mechanism must be present to form ethanol, which was so far not accounted for by the overall reaction scheme in Figure 1.

To verify the stability of the desired product 1,2-PDO under the applied reaction conditions, a 20 wt % 1,2-PDO solution was used as a reactant to investigate its stability under typical hydrogenolysis conditions of 220 °C and 25 bar hydrogen pressure using the Ru−Cu/CNT catalyst. Figure 13 shows the temporal 1,2-PDO conversion and the various product yields and selectivities. Both 1,2-PDO conversion and the yield of decomposition products increased linearly over time. Except for the dehydrogenation product acetol, which is formed in only very small amounts after 300 min, all products were formed from the very beginning of the reaction. While the formation of n-propanol via hydrogenolysis was expected, the other decomposition products were not mentioned in the original reaction network. The formation of acetol suggests a reversibility of the reaction, which was indicated by simulations done by Gatti et al.[12] but not experimentally verified in the literature. Additionally, ethanol, methane, and ethane were expected to be products of the C−C cleavage pathway rather than the 1,2-PDO pathway. However, since ethylene glycol was found to be stable under hydrogenolysis conditions (Figure S12), the presence of ethanol, methane, and ethane now explains why ethanol was detected in previous experiments (see Figure 9). This also means that the already complex network of possible reaction pathways becomes even more multifaceted. Additionally, the expected decomposition of n-propanol to propane was not observed.

We suggest an additional decomposition pathway for 1,2-PDO (Figure 14), which is analogous to the C−C-cleavage of glycerol to ethylene glycol. In the first step, 1,2-PDO undergoes a C−C-cleavage to produce ethanol and methanol. In the second step, methanol is hydrogenated to produce methane. While this reaction is mechanistically plausible, no methanol is found in the reaction solution. This suggests that all of the methanol must have been converted to methane. This is supported by the fact that even in the reaction where ethylene glycol is formed no methanol could be detected (see Figure 9).

A second 1,2-PDO stability experiment at optimized hydrogenation conditions of 145 °C was conducted, and no 1,2-PDO conversion was observed, as shown in Figure S13. The fact that 1,2-PDO remains stable at these conditions indicates that a hydrogenation at lower temperatures not only achieves quantitative acetol conversion and completely suppresses ethylene glycol formation but also prevents subsequent hydrogenolysis of 1,2-PDO.

Temperature Variation for Determination of the Activation Energy

The influence of the reaction temperature on the overall reaction rate of glycerol hydrogenolysis was investigated by varying the reaction temperature from 200 to 240 °C in 10 °C steps. The corresponding temporal glycerol concentration, including the linear regression to determine the reaction rate and temporal conversion graphs, is shown in Figure 15. All graphs show a decreasing concentration of glycerol over time. However, the rate of glycerol consumption increases with increasing temperature according to the Arrhenius law. The slope of the linear fit, determining the reaction rate, increases 10-fold from 0.00022 mol L^{-1} min^{-1} at 200 °C to 0.0021 mol L^{-1} min^{-1} at 240 °C.

Figure 16 shows that an increase in reaction temperature not only affects the kinetics of the glycerol hydrogenolysis reaction but also favors more undesired side reactions like C−C bond cleavage leading to ethylene glycol and glycerol reforming. The corresponding temporal profiles of product yields are shown in Figure S14. While an increase in temperature leads to higher glycerol conversion (37.6%) and 1,2-PDO yield (19.7%) at 240 °C, 1,2-PDO selectivity drops above 230 °C, whereas the selectivity increases significantly from 27.8% at 200 °C to 57.5% at 210 °C, then rises slowly until reaching a maximum of 64.9% at 230 °C. After that, it decreases to 52.4% at 240 °C. The reason for the low selectivity at 200 °C is that exothermic ethylene glycol formation is favored over 1,2-PDO formation at lower temperatures. At higher temperatures, endothermic dehydration is favored, leading to more acetol formation, and the formed 1,2-PDO undergoes consecutive hydrogenolysis to n-propanol (as shown in previous experiments). A reaction temperature of 230 °C seems to be a sweet spot for glycerol hydrogenolysis, as it favors C−O activation over C−C activation but still prevents glycerol reforming.

In addition to the optimization of the reaction conditions, the temperature variation also enables a graphical determi-

https://doi.org/10.1021/acssuschemeng.6c02083
ACS Sustainable Chem. Eng. XXXX, XXX, XXX−XXX

nation of the activation energy using an Arrhenius plot (Figure 17). The reaction rate ln(k) increases as the reaction temperature increases. Figure 17a shows the Arrhenius plot for the overall glycerol consumption and results in an activation energy of 121.75 kJ mol^{-1}. This value is similar to that determined for a Cu/Zn:Cr/Zr mixed metal oxide catalyst (131.88 kJ mol^{-1}) in the literature.[35] Figure 17b shows the Arrhenius plot for the 1,2-PDO pathway, yielding an activation energy of 154 kJ mol^{-1}. The activation energy for the ethylene glycol pathway is 60 kJ mol^{-1}, and the corresponding Arrhenius energy is shown in Figure S15. A table of the starting and final pathway concentrations is provided in the Supporting Information (Table S4).

Kinetic Modeling of the Glycerol Hydrogenolysis

The kinetic experiments enable the construction of a kinetic model of the glycerol hydrogenolysis based on the reaction rate (eqs 10,11). eq 10 describes the 1,2-PDO pathway, while eq 11 describes the undesired ethylene glycol pathway. The more detailed methodology is shown in the Supporting Information (section: Kinetic modeling of the glycerol hydrogenolysis).

$$r_1 = k_{0,1} \cdot e^{(-E_{A,1}/R \cdot T)} \cdot C_G^{n_{1,Gly}} \cdot C_H^{n_{1,H}} \quad (10)$$

$$r_2 = k_{0,2} \cdot e^{(-E_{A,2}/R \cdot T)} \cdot C_G^{n_{2,Gly}} \cdot C_H^{n_{2,H}} \quad (11)$$

Where r_i values are the reaction rates, $k_{0,i}$ values are the pre-exponential factors, $E_{A,i}$ values are the activation energies, T is the temperature, C_j are the molar concentrations, and $nj_{,i}$ is the reaction rate order in reaction i with respect to species j. The complete methodology is shown in the Supporting Information in the section "Kinetic modeling of glycerol hydrogenolysis". The parameter estimates are listed in Table 3. For the kinetic model, only the experiments using 25, 30, 40, and 50 bar partial hydrogen pressure were included, due to catalyst surface saturation below 25 bar and the fact that all other variation experiments were conducted at 50 bar hydrogen pressure.

The estimated reaction orders for the 1,2-PDO pathway of 1.17 for glycerol and −1.36 for hydrogen are very close to the experimentally determined reaction order of 1.04 for glycerol and −1.31 for hydrogen. The same is true for the estimated activation energy of 149 kJ mol^{-1}, which is similar to the experimentally determined value of 154 kJ mol^{-1}. The estimated pre-exponential factor of 4.13×10^9 ($M^{(1-n)}$/Min) is slightly lower compared to the experimentally determined one of 1.60×10^{10} ($M^{(1-n)}$/Min), however, the experimentally determined value still falls within the confidence intervals. For the ethylene glycol pathway, the estimated and experimentally determined parameters are also similar. Comparing the parametrized kinetic models with experimental data (as shown in Figures S16−S18) confirms that the models reliably reproduce the observed reaction behavior.

CONCLUSIONS

The kinetics of glycerol hydrogenolysis to 1,2-PDO, as well as the competing C−C-cleavage reaction to ethylene glycol and methanol, were studied. The reaction conditions were optimized to achieve higher 1,2-PDO yield by increasing glycerol conversion. Additionally, the individual subreactions comprising the glycerol hydrogenolysis reaction network were also investigated. This resulted in the addition of a new 1,2-PDO decomposition pathway to the reaction network. Furthermore, the knowledge about reaction kinetics revealed a new approach to glycerol hydrogenolysis with a promising higher yield and selectivity. Kinetic experiments were conducted by varying the initial glycerol concentration (2.5 to 80%), the initial hydrogen partial pressure (10 to 50 bar), and the reaction temperature (200 to 240 °C). Hydrogen pressure significantly influenced glycerol conversion; the reaction exhibited kinetically limited behavior at low pressures and reactant surface adsorption limitation at high pressures. Optimizing the reaction conditions resulted in 20.7% glycerol conversion, a 14.6% 1,2-PDO yield, 76.5% selectivity at 220 °C, 25 bar hydrogen pressure, and 20 wt % glycerol.

Investigating the individual subreactions revealed that dehydration to acetol is the rate-determining step and that acetol can be quantitatively hydrogenated already at lower reaction temperatures of only 145 °C. Additionally, it was demonstrated that ethylene glycol decomposition does not produce ethanol; instead, ethanol results from the decomposition of 1,2-PDO. A separate approach for the hydrogenolysis of glycerol was implemented as a proof of concept, and the successful suppression of ethylene glycol formation and subsequent hydrogenolysis to monoalcohols demonstrated its effectiveness. This was achieved by first dehydrating glycerol to acetol under nitrogen and then hydrogenating the acetol at lower temperatures to 1,2-PDO, resulting in an almost perfect 1,2-PDO selectivity >99%. Additionally, based on the derived kinetic parameters, a simple kinetic model could be established.

ASSOCIATED CONTENT

Data Availability Statement

Research data is available/will be made available after official publication (10.15480/882.16745).

Supporting Information

The Supporting Information is available free of charge at https://pubs.acs.org/doi/10.1021/acssuschemeng.6c02083.

Sample digestion for ICP-OES, details and PID of the experimental setup, HPLC calibration, plot for catalyst loading variation, plots for reactants influence on kinetics, and product stability (PDF)

AUTHOR INFORMATION

Corresponding Author

Jakob Albert − *Institute of Technical and Macromolecular Chemistry, University of Hamburg, Hamburg 20146, Germany*; orcid.org/0000-0002-3923-2269; Email: jakob.albert@uni-hamburg.de

Authors

Piet Hassenstein − *Institute of Technical and Macromolecular Chemistry, University of Hamburg, Hamburg 20146, Germany*

Daniel Niehaus − *Institute of Technical and Macromolecular Chemistry, University of Hamburg, Hamburg 20146, Germany*

Nazanin Taherkhani − *Institute of Technical and Macromolecular Chemistry, University of Hamburg, Hamburg 20146, Germany*

Jan-Dominik H. Krueger − *Institute of Technical and Macromolecular Chemistry, University of Hamburg, Hamburg 20146, Germany*

https://doi.org/10.1021/acssuschemeng.6c02083
ACS Sustainable Chem. Eng. XXXX, XXX, XXX−XXX

Dorothea Voß − *Institute of Technical and Macromolecular Chemistry, University of Hamburg, Hamburg 20146, Germany;* orcid.org/0000-0003-1693-8012
Dominique Lumpp − *Institute of Technical and Macromolecular Chemistry, University of Hamburg, Hamburg 20146, Germany;* orcid.org/0009-0008-4083-0355
Baldur Schroeter − *Institute of Thermal Separation Processes, Hamburg University of Technology, Hamburg 21073, Germany;* orcid.org/0000-0002-2577-055X
Leandros Paschalidis − *Institute of Process Systems Engineering, Hamburg University of Technology, Hamburg 21073, Germany*
Irina Smirnova − *Institute of Thermal Separation Processes, Hamburg University of Technology, Hamburg 21073, Germany;* orcid.org/0000-0003-4503-4039
Mirko Skiborowski − *Institute of Process Systems Engineering, Hamburg University of Technology, Hamburg 21073, Germany;* orcid.org/0000-0001-9694-963X

Complete contact information is available at: https://pubs.acs.org/10.1021/acssuschemeng.6c02083

Notes

The authors declare no competing financial interest.

■ ACKNOWLEDGMENTS

This project was funded by the Deutsche Forschungsgemeinschaft (DFG, German Research Foundation) −SFB 1615−503850735. We want to acknowledge Bo Elfers and his team at the Central Analytics of TUHH for performing the ICP-OES measurements. Special thanks to Philipp Kampe for installing the reactor setup used in this study and to Nick Herrmann for many helpful discussion regarding this project.

■ REFERENCES

(1) Behr, A.; Seidensticker, T.. Das Koppelprodukt Der Oleochemie. In *EinfüHrung in Die Chemie Nachwachsender Rohstoffe: Vorkommen, Konversion, Verwendung*; Springer: Berlin Heidelberg: Berlin, Heidelberg, 2018; pp 85−105..
(2) Kraleva, E.; Palcheva, R.; Dimitrov, L.; Armbruster, U.; Brückner, A.; Spojakina, A. Solid Acid Catalysts for Dehydration of Glycerol to Acrolein in Gas Phase. *J. Mater. Sci.* **2011**, *46* (22), 7160−7168.
(3) Dietz, D.; Zeng, A.-P. Efficient Production of 1,3-Propanediol from Fermentation of Crude Glycerol with Mixed Cultures in a Simple Medium. *Bioprocess Biosyst. Eng.* **2014**, *37* (2), 225−233.
(4) Ma, F.; Hanna, M. A. Biodiesel Production: A review1Journal Series #12109, Agricultural Research Division, Institute of Agriculture and Natural Resources, University of Nebraska−Lincoln.1. *Bioresour. Technol.* **1999**, *70* (1), 1−15.
(5) Christoph, R.; Schmidt, B.; Steinberner, U.; Dilla, W. Glycerol. In *Ullmann's Encyclopedia of Industrial Chemistry*; Wiley-VCH Verlag GmbH & Co. KGaA: Weinheim, Germany, 2000; ..
(6) Modvig, A.; Kumpidet, C.; Riisager, A.; Albert, J. Ru-Doped Wells−Dawson Polyoxometalate as Efficient Catalyst for Glycerol Hydrogenolysis to Propanediols. *Materials* **2019**, *12* (13), 2175.
(7) Oliveira, G. N.; Barbosa, N. C.; Araújo, F. C.; Souza, P. H. G.; Soares, A. V. H.; Peixoto, F. C.; Carneiro, J. W. M.; Passos, F. B. Conversion of Glycerine into 1,2-Propanediol for Industrial Applications. In *Jatropha, Challenges for a New Energy Crop*; Springer Singapore: Singapore, 2019; pp 383−414..
(8) Główka, M.; Krawczyk, T. New Trends and Perspectives in Production of 1,2-Propanediol. *ACS Sustain. Chem. Eng.* **2023**, *11* (19), 7274−7287.
(9) F., Matter In *Current Developments in Biotechnology and Bioengineering*; A., Pandey, H. H., Ngo, W., Guo, S., Varjani, D. C. W., Tsang, Eds.; Elsevier, 2023; pp i−iii. DOI: .
(10) Gatti, M.; Pompeo, F.; Nichio, N.; Santori, G. Crude Glycerol Hydrogenolysis to Bio-Propylene Glycol: Effect of Its Impurities on Activity, Selectivity and Stability. *Processes* **2023**, *11* (6), 1731.
(11) Dasari, M. A.; Kiatsimkul, P.-P.; Sutterlin, W. R.; Suppes, G. J. Low-Pressure Hydrogenolysis of Glycerol to Propylene Glycol. *Appl. Catal. Gen.* **2005**, *281* (1−2), 225−231.
(12) Gatti, M. N.; Perez, F. M.; Santori, G. F.; Pompeo, F. Mechanism Analysis and Chemical Equilibrium Modelling for Liquid Phase Glycerol Hydrogenolysis. *Chem. Thermodyn. Therm. Anal.* **2025**, *18*, 100186.
(13) Coll, D.; Delbecq, F.; Aray, Y.; Sautet, P. Stability of Intermediates in the Glycerol Hydrogenolysis on Transition Metal Catalysts from First Principles. *Phys. Chem. Chem. Phys.* **2011**, *13* (4), 1448−1456.
(14) Miyazawa, T.; Kusunoki, Y.; Kunimori, K.; Tomishige, K. Glycerol Conversion in the Aqueous Solution under Hydrogen over Ru/C + an Ion-Exchange Resin and Its Reaction Mechanism. *J. Catal.* **2006**, *240* (2), 213−221.
(15) Wang, J.; Shen, S.; Li, B.; Lin, H.; Yuan, Y. Ruthenium Nanoparticles Supported on Carbon Nanotubes for Selective Hydrogenolysis of Glycerol to Glycols. *Chem. Lett.* **2009**, *38* (6), 572−573.
(16) Feng, J.; Fu, H.; Wang, J.; Li, R.; Chen, H.; Li, X. Hydrogenolysis of Glycerol to Glycols over Ruthenium Catalysts: Effect of Support and Catalyst Reduction Temperature. *Catal. Commun.* **2008**, *9* (6), 1458−1464.
(17) Furikado, I.; Miyazawa, T.; Koso, S.; Shimao, A.; Kunimori, K.; Tomishige, K. Catalytic Performance of Rh/SiO2 in Glycerol Reaction under Hydrogen. *Green Chem.* **2007**, *9* (6), 582.
(18) Raso, R.; García, L.; Ruiz, J.; Oliva, M.; Arauzo, J. Aqueous Phase Hydrogenolysis of Glycerol over Ni/Al-Fe Catalysts without External Hydrogen Addition. *Appl. Catal. B Environ.* **2021**, *283*, 119598.
(19) Perosa, A.; Tundo, P. Selective Hydrogenolysis of Glycerol with Raney Nickel. *Ind. Eng. Chem. Res.* **2005**, *44* (23), 8535−8537.
(20) Yin, A.-Y.; Guo, X.-Y.; Dai, W.-L.; Fan, K.-N. The Synthesis of Propylene Glycol and Ethylene Glycol from Glycerol Using Raney Ni as a Versatile Catalyst. *Green Chem.* **2009**, *11* (10), 1514.
(21) Oberhauser, W.; Evangelisti, C.; Jumde, R. P.; Psaro, R.; Vizza, F.; Bevilacqua, M.; Filippi, J.; Machado, B. F.; Serp, P. Platinum on Carbonaceous Supports for Glycerol Hydrogenolysis: Support Effect. *J. Catal.* **2015**, *325*, 111−117.
(22) D'Hondt, E.; Van De Vyver, S.; Sels, B. F.; Jacobs, P. A. Catalytic Glycerol Conversion into 1,2-Propanediol in Absence of Added Hydrogen. *Chem. Commun.* **2008**, *45*, 6011.
(23) Wawrzetz, A.; Peng, B.; Hrabar, A.; Jentys, A.; Lemonidou, A. A.; Lercher, J. A. Towards Understanding the Bifunctional Hydrodeoxygenation and Aqueous Phase Reforming of Glycerol. *J. Catal.* **2010**, *269* (2), 411−420.
(24) Zhao, H.; Zheng, L.; Li, X.; Chen, P.; Hou, Z. Hydrogenolysis of Glycerol to 1,2-Propanediol over Cu-Based Catalysts: A Short Review. *Catal. Today* **2020**, *355*, 84−95.
(25) Bienholz, A.; Schwab, F.; Claus, P. Hydrogenolysis of Glycerol over a Highly Active CuO/ZnOcatalyst Prepared by an Oxalate Gel Method: Influence of Solvent and Reaction Temperature on Catalyst Deactivation. *Green Chem.* **2010**, *12* (2), 290−295.
(26) Guo, L.; Zhou, J.; Mao, J.; Guo, X.; Zhang, S. Supported Cu Catalysts for the Selective Hydrogenolysis of Glycerol to Propanediols. *Appl. Catal. Gen.* **2009**, *367* (1−2), 93−98.
(27) Wang, S.; Yin, K.; Zhang, Y.; Liu, H. Glycerol Hydrogenolysis to Propylene Glycol and Ethylene Glycol on Zirconia Supported Noble Metal Catalysts. *ACS Catal.* **2013**, *3* (9), 2112−2121.
(28) Maris, E. P.; Davis, R. J. Hydrogenolysis of Glycerol over Carbon-Supported Ru and Pt Catalysts. *J. Catal.* **2007**, *249* (2), 328−337.

(29) Sherbi, M.; Wesner, A.; Wisniewski, V. K.; Bukowski, A.; Velichkova, H.; Fiedler, B.; Albert, J. Superior CNT-Supported Bimetallic RuCu Catalyst for the Highly Selective Hydrogenolysis of Glycerol to 1,2-Propanediol. *Catal. Sci. Technol.* **2021**, *11* (20), 6649−6653.
(30) Torres, A.; Roy, D.; Subramaniam, B.; Chaudhari, R. V. Kinetic Modeling of Aqueous-Phase Glycerol Hydrogenolysis in a Batch Slurry Reactor. *Ind. Eng. Chem. Res.* **2010**, *49* (21), 10826−10835.
(31) Vasiliadou, E. S.; Lemonidou, A. A. Kinetic Study of Liquid-Phase Glycerol Hydrogenolysis over Cu/SiO2 Catalyst. *Chem. Eng. J.* **2013**, *231*, 103−112.
(32) Gabrysch, T.; Muhler, M.; Peng, B. The Kinetics of Glycerol Hydrodeoxygenation to 1,2-Propanediol over Cu/ZrO2 in the Aqueous Phase. *Appl. Catal. Gen.* **2019**, *576*, 47−53.
(33) Pandhare, N. N.; Pudi, S. M.; Mondal, S.; Pareta, K.; Kumar, M.; Biswas, P. Development of Kinetic Model for Hydrogenolysis of Glycerol over Cu/MgO Catalyst in a Slurry Reactor. *Ind. Eng. Chem. Res.* **2018**, *57* (1), 101−110.
(34) Ardila A, A. N.; Arriola-Villaseñor, E.; Barrera-Zapata, R.; Hernández, J.; Fuentes, G. A. Kinetic Study of Liquid-Phase Glycerol Hydrodeoxygenation into 1,2-Propanediol over CuPd/TiO_2-Na. *ACS Omega* **2023**, *8* (17), 14907−14914.
(35) Sharma, R. V.; Kumar, P.; Dalai, A. K. Selective Hydrogenolysis of Glycerol to Propylene Glycol by Using Cu:Zn:Cr:Zr Mixed Metal Oxides Catalyst. *Appl. Catal. Gen.* **2014**, *477*, 147−156.
(36) Chiu, C.; Dasari, M. A.; Suppes, G. J.; Sutterlin, W. R. Dehydration of Glycerol to Acetol via Catalytic Reactive Distillation. *AIChE J.* **2006**, *52* (10), 3543−3548.
(37) Soares, A. V.-H.; Perez, G.; Passos, F. B. Alumina Supported Bimetallic Pt−Fe Catalysts Applied to Glycerol Hydrogenolysis and Aqueous Phase Reforming. *Appl. Catal. B Environ.* **2016**, *185*, 77−87.
(38) Ma, L.; He, D. Hydrogenolysis of Glycerol to Propanediols Over Highly Active Ru−Re Bimetallic Catalysts. *Top. Catal.* **2009**, *52* (6−7), 834−844.
(39) Feng, J.; Zhang, Y.; Xiong, W.; Ding, H.; He, B. Hydrogenolysis of Glycerol to 1,2-Propanediol and Ethylene Glycol over Ru-Co/ZrO2 Catalysts. *Catalysts* **2016**, *6* (4), 51.
(40) Feng, J.; Xu, B.; Liu, D. R.; Xiong, W.; Wang, J. B. Performances of Titania-Supported Ru-Based Bimetallic Catalysts in Glycerol Hydrogenolysis Reaction. *Adv. Mater. Res.* **2013**, *791−793*, 12−15.
(41) Gatti, M. N.; Perez, F. M.; Santori, G. F.; Nichio, N. N.; Pompeo, F. Heterogeneous Catalysts for Glycerol Biorefineries: Hydrogenolysis to 1,2-Propylene Glycol. *Materials* **2023**, *16* (9), 3551.
(42) Gallegos-Suarez, E.; Guerrero-Ruiz, A.; Rodriguez-Ramos, I.; Arcoya, A. Comparative Study of the Hydrogenolysis of Glycerol over Ru-Based Catalysts Supported on Activated Carbon, Graphite, Carbon Nanotubes and KL-Zeolite. *Chem. Eng. J.* **2015**, *262*, 326−333.
(43) Lumpp, D.; Shaikh, S.; Riebesehl, F.; Ruhmlieb, C.; Kruber, K.; Schroeter, B.; Smirnova, S.; Skiborowski, M.; Fiedler, B.; Albert, J. Multifunctional Carbon-Nanotube Supported Catalysts for Efficient Glycerol Hydrogenolysis to 1,2-Propanediol. *ChemChatChem.* **2026**, *18* (5), No. e01748.
(44) Fick, A. Ueber Diffusion. *Ann. Phys.* **1855**, *170* (1), 59−86.
(45) Sander, R. Compilation of Henry's Law Constants (Version 5.0.0) for Water as Solvent. *Atmospheric Chem. Phys.* **2023**, *23* (19), 10901−12440.
(46) Roy, D.; Subramaniam, B.; Chaudhari, R. V. Aqueous Phase Hydrogenolysis of Glycerol to 1,2-Propanediol without External Hydrogen Addition. *Catal. Today* **2010**, *156* (1−2), 31−37.

https://doi.org/10.1021/acssuschemeng.6c02083
ACS Sustainable Chem. Eng. XXXX, XXX, XXX−XXX